SIMULATION OF SCATTERING EFFECTS OF MARINE ORGANISMS ON ACTIVE SONAR RETURNS

Sergey Simakov(1) and Zhi Yong Zhang(1)

(1) Maritime Operations Division, DSTO, PO Box 1500, Edinburgh SA 5111, Australia

Abstract

Marine organisms with gas inclusions, such as fish with swim bladders and bubble-carrying plankton, can scatter sound strongly thus contributing to volume reverberation of an active sonar and possibly introducing distortion to its pulses. Numerical evaluation of scattering effects from these objects is often based on reduction of their shapes to simple geometries, such as spheres or cylinders. In this work we use a viscous compressible spherical shell model with a gas inclusion to obtain a parameterisation of the frequency dependence of the scattering cross section of individual scatterers in terms of their effective size and material properties. We consider the range of sonar frequencies and scatterer sizes for which the contribution of non-monopole spherical modes becomes significant. Graphical interfacing of access to model parameters is discussed and an assessment of the characteristics of the echo returns from an ensemble of scatterers in frequency and time domains is given.

Introduction

Populations of marine organisms with inner gas cavities, such as fish with swim bladders or bubble carrying plankton, can scatter sound strongly thus contributing to volume reverberation of an active sonar. Scattering properties of such creatures have been investigated in many studies (e.g. [1-10]). Qualitative estimation of the associated scattering effects is often based on the reduction of the shapes of the scatterers to simple geometries, which in many cases can be justified by the variety of shapes and orientations. In this paper, in order to simulate acoustical responses of individual objects, we employ the model developed in [7, 10]. The scatterer in this model can be described as a compressible viscous spherical shell with a gas inclusion. The scattering cross section of such a shell depends on its size and material properties, and is a nontrivial function of frequency. We consider the range of sonar frequencies and scatterer sizes for which the contribution of non-monopole spherical modes becomes significant. We also discuss graphical interfacing to the model's input parameters and give an assessment of the characteristics of scattering responses in frequency and time domain.

The model

Consider a sound pulse with plane wave front propagating in the positive z-direction

$$u_0(z,t) = f(z-ct), \tag{1}$$

where $u_0(z, t)$ is pressure disturbance, t is time and c is the speed of sound in water. This pulse can be written as a superposition of plane harmonic waves

$$u_0(z,t) = \int_{-\infty}^{\infty} e^{i\frac{\omega}{c}(z-ct)} U_p(\omega)\, d\omega,$$

where $U_p = F(\omega / c)/(2\pi c)$ and $F(k)$ is the Fourier transform $f(z) \to F(k)$. If there is a scatterer centred at the origin, the total field at point $\mathbf{r}$ is

$$u(\mathbf{r},t) = \int_{-\infty}^{\infty} e^{-i\omega t} U_p(\omega) \left[e^{i\frac{\omega}{c}z} + u_s(\mathbf{r},\omega) \right] d\omega.$$

The term $u_s(\mathbf{r},\omega)$ describes the scattering component given in the axially symmetric case for positive ω by

$$u_s = \sum_m P_m(\cos\theta) A_m(\omega) h_m^{(1)}(kr),$$

where $k=\omega/c$, $r=|\mathbf{r}|$, $h_m^{(1)}(\xi)$ is the spherical Hankel function of the first kind, i.e.

$$\begin{aligned} h_m^{(1)}(\xi) &\equiv \sqrt{\frac{\pi}{2\xi}} H_{m+1/2}^{(1)}(\xi) \\ &= \xi^m \left(-\frac{1}{\xi}\frac{d}{d\xi} \right)^{m+1} e^{i\xi}, \end{aligned} \tag{2}$$

and P_m are Legendre polynomials. For negative frequencies we have

$$u_s(\mathbf{r},-\omega) = u_s^*(\mathbf{r},\omega).$$

Coefficients $A_m(\omega)$ depend on the scatterer. Construction of $A_m(\omega)$ for a viscous compressible shell with a gas inclusion was reported in [7, 10]. Here we employed the technique described in [7] with the following modification: *the compressional and the shear fields in the viscous shell are expressed directly in terms of the spherical Hankel functions* $h_m^{(1)}$ *and* $h_m^{(2)}$. This approach allowed us to separate very large and very small terms, which appear in combination in the spherical Bessel and Neumann functions, j_m and n_m, when the frequency is

large. Appropriately rescaling the resulting system for the expansion coefficients and explicitly solving with respect to $A_m^{(1)} (\equiv A_m)$, we obtain a fast and stable procedure for computation of the scattering field in the frequency domain. The parameters which govern the scattering properties of the model are as follows: water density ρ_1, shell material density ρ_2, gas density ρ_3, speeds of sound in water (c), the shell (c_{sh}), and the gas (c_g), viscosity parameter ξ of the shell material, and the inner and outer shell radii r_0 and R.

If ω is fixed and positive and $kr \gg 1$, the scattering term can be written using (2), or the general asymptotic expansion of the Hankel functions, as

$$u_s \cong \sum_m (-i)^{m+1} P_m(\cos\theta) A_m(\omega) \frac{e^{ikr}}{kr}. \qquad (3)$$

If our pulse is confined to a frequency band centred at ω_0, i.e.

$$|\omega - \omega_0| < \Delta\omega, \qquad (4)$$

then, in the time domain, the scattering component takes the form

$$v(\mathbf{r},t) \cong \mathrm{Re} \sum_m (-i)^{m+1} \frac{P_m(\cos\theta)}{\pi r} Q_m(r-ct),$$

where

$$Q_m(\xi) = \int_{\omega_0-\Delta\omega}^{\omega_0+\Delta\omega} e^{i\frac{\omega}{c}\xi} F(\omega/c) \frac{A_m(\omega)}{\omega} d\omega. \qquad (5)$$

If there is a cloud of N scatterers, the combined response in the single scattering approximation, in which we assume that the response of each scatterer is not affected by the presence of the other scatterers, is given by

$$v \cong \mathrm{Re} \sum_{l=1}^{N} \sum_m (-i)^{m+1} \frac{P_m(\cos\theta)}{\pi r} \times Q_m\left(\left|\mathbf{r}-\mathbf{R}_l\right| + (\mathbf{R}_l \cdot \mathbf{e}_z) - ct\right), \qquad (6)$$

where $\mathbf{R}_l$ is the location of scatterer l ($\mathbf{R}_1 = \mathbf{0}$) and we assume that $r\omega_0 / c \gg 1$. In the far-field, where

$$\max_l |\mathbf{R}_l|^2 / r \ll 2\pi c / \omega_o, \qquad (7)$$

the argument of Q_m can be reduced to a simpler expression $r - \mathbf{R}_l(\mathbf{e}_r - \mathbf{e}_z) - ct$.

Evaluation of (5) in the general case requires sampling of $f(z)$ with a proper rate and computation of $A_m(\omega)$ for the corresponding frequencies. Fast numerical integration can be carried out using the Fast Fourier Transform. An analytic treatment of (5) is possible if $\Delta\omega$ is small and $A_m(\omega)$ varies slowly in (4), in which case $A_m(\omega)/\omega$ in the integrand can be replaced with its value at ω_0. If, for example,

$$f(z) = \cos(az) e^{-z^2/b^2}, \qquad (8)$$

then this approach gives

$$Q_m(\xi) = \frac{\pi c A_m(\omega_0)}{\omega_0} e^{i\frac{\omega_0}{c}\xi} e^{-\frac{\xi^2}{b^2}},$$

where $\omega_0 \equiv ac$. Note that parameters a and b in (8) allow us to control the carrier frequency and the duration of the pulse, which at t=0 is localized near the line z = 0. Interpretation of the solution will require considering it at a receiver during a time interval associated with the arrival of the main pulse and the returns from the scatterers.

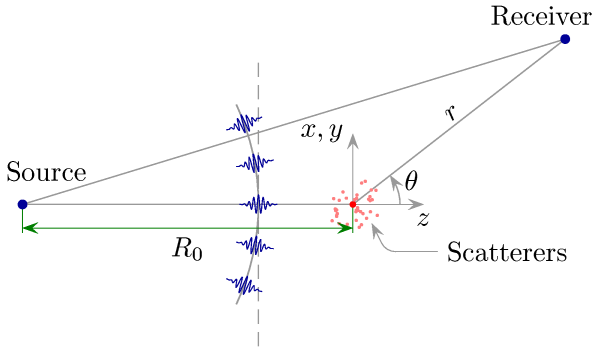

Figure 1. Scattering geometry

Consider now a spherical propagating pulse sketched in Figure 1. We will assume for simplicity that the pulse originates from an omnidirectional source centred at $z_0 = -R_0$. The space-time dependence of the propagating field can be written as

$$S_0(R,t) = \frac{q(R-ct)}{R}, \qquad (9)$$

where R is the distance to the centre of the source. If R_0 is large so that the far-field condition is satisfied

$$\max_l |\hat{\mathbf{R}}_l|^2 / R_0 \ll 2\pi c / \omega_0, \qquad (10)$$

where $\hat{\mathbf{R}}_l$ is the projection of $\mathbf{R}_l$ on the (x, y) plane, then locally at the origin and near the scatterers the field (9) can be approximated by a one-dimensional pulse $f(z–ct)$, which can be used in formula (5) for evaluation of the scattering field. The far-field requirement (10) can be somewhat relaxed to just $R_0 \gg \max_l |\mathbf{R}_l|$ if in (6), instead of $(\mathbf{R}_l \cdot \mathbf{e}_z)$, we use

$$\delta r_l \equiv \left|\mathbf{R}_l + R_0 \mathbf{e}_z\right| - R_0. \qquad (11)$$

The relationship between q and f is as follows

$$q(\xi) = R_0 f(\xi - R_0). \tag{12}$$

We will use here f and R_0 as input data and relation (12) as a reconstruction formula for $q(\xi)$. Expressed in terms of f, equation (9) takes the form

$$S_0(R,t) = \frac{R_0}{R} f(R - ct - R_0). \tag{13}$$

Formulae (6) and (13) describe the scattered and the primary field in terms of the input signal f, the parameters R_0, $\{\mathbf{R}_l\}$ and the receiver's position **r.**

We provide below the far-field expressions for a receiver positioned on the z-axis.

Case (a): **r** = (0, 0, – | z |) corresponds to backscattering. The scattering term takes the form

$$v \cong \mathrm{Re} \sum_{l=1}^{N} \sum_{m} (-i)^{m+1} \frac{P_m(\cos\theta)}{\pi |z|} \times Q_m(|z| + 2\mathbf{R}_l \cdot \mathbf{e}_z - ct). \tag{14}$$

During arrival of these returns at the receiver the primary field makes no contribution to the signal, i.e. $S(R, t) = 0$.

Case (b): **r**=(0, 0, $z > 0$) corresponding to the forward scattering yields

$$v \cong N\,\mathrm{Re} \sum_{m} (-i)^{m+1} \frac{P_m(\cos\theta)}{\pi z} Q_m(z - ct). \tag{15}$$

The scattered field arrives at the receiver together with the primary field which is given by

$$S_0(R,t) = \frac{R_0 f(z - ct)}{z + R_0}. \tag{16}$$

Target strength

The ability of an object to scatter wave energy in a certain direction is described in the frequency domain by the differential scattering cross section defined as

$$\sigma_d \equiv r^2 I_s(\theta) / I_0, \tag{17}$$

where I_0 is the intensity of the incident monochromatic plane wave and $I_s(\theta)$ is the far-field intensity of the scattered wave in the direction θ. Substitution of (3) into (17) gives

$$\sigma_d = \frac{1}{k^2} \left| \sum_{m} (-i)^m A_m(\omega) P_m(\cos\theta) \right|^2. \tag{18}$$

Acoustic scattering length L (e.g. [11, page 237]) and the target strength TS, for which we have

$$|L| = \sqrt{\sigma_d} \quad \text{and} \quad \mathrm{TS} \equiv 10 \log(\sigma_d / 1\mathrm{m}^2)$$

are the concepts closely related to σ_d.

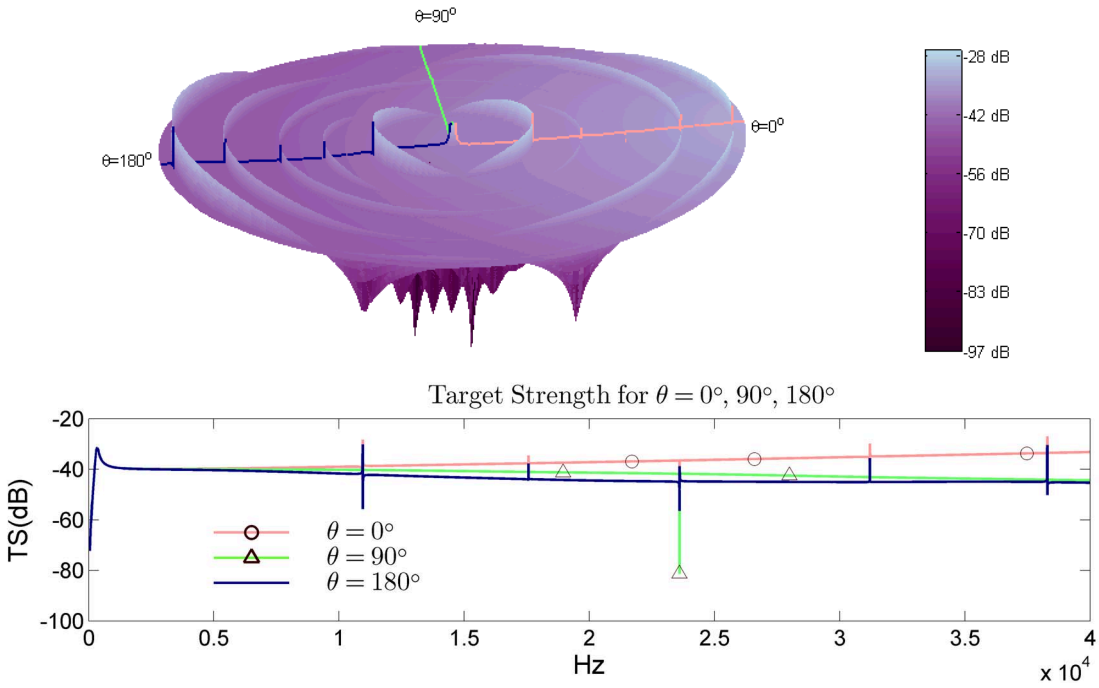

Figure 2. Spectral and angular variability of target strength.

We can see from (18) that target strength depends on both the scattering direction θ and the frequency ω of incident wave. Figure 2, in which the frequency is used as a polar radius and θ as a polar angle, illustrates both spectral and angular variability of target strength. Input parameters used in this computation are given in the Table 1.

ρ_1	ρ_2	ρ_3
1000 kg/m^3	1004.6 kg/m^3	1.26 kg/m^3
c_w	c_{sh}	c_g
1500 m/s	1500 m/s	330 m/s
ξ	r_0	R
25 poise	0.01 m	0.06 m

Table 1. Parameters of an individual scatterer

We took into account only the contribution of the modes m from 0 to 10, since, in the range of frequencies under consideration and for these values of shell parameters, the influence of the modes with $m > 10$ can be safely neglected. The comparison of the target strengths obtained using monopole and full mode solutions in Figure 3 shows, that we have to depart from the *monopole mode rationale* at higher frequencies.

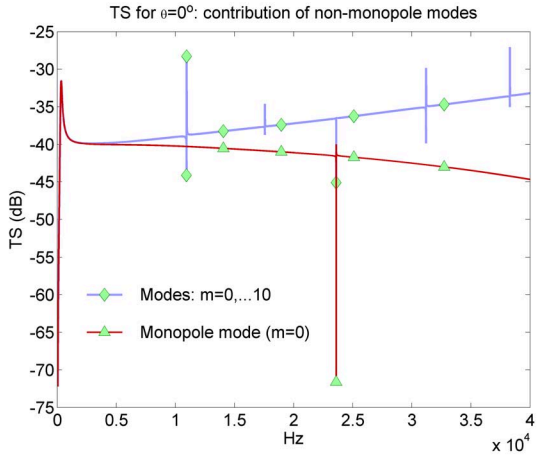

Figure 3. Monopole and full mode solution

Note that some prominent spectral features of the amplitude $A_m(\omega)$ may not be noticeable in certain directions. For example, $A_1(\omega)$ corresponding to the configuration shown in the table has a resonance near 10.943 kHz, but since $P_1(\cos\theta)$ vanishes at $\theta=\pi/2$, there will be no contribution of mode m=1 to target strength in the direction perpendicular to the wave vector of the incident wave.

As we indicated earlier, the model has 9 input parameters. Since constructing a simple analytic expression for the model's target strength is not feasible, we provided access to these parameters via a graphical user interface. The tool shown in Figure 4 allows one to observe almost instantaneously how changes of their values affect the plot of the target strength. To facilitate fitting, measurement data for a set of frequencies can be loaded and displayed. It is understandable that the shape of most real marine organisms is far from spherical. However, the variety of shapes and orientations of the scatterers justifies to some extent introduction of scatterer's equivalent spherical radius and its use for qualitative estimates.

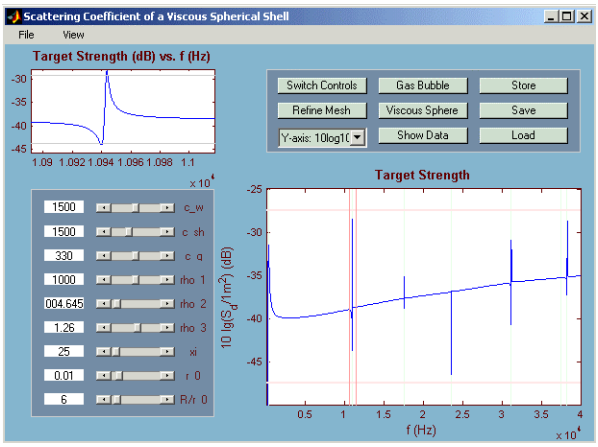

Figure 4. GUI to input parameters

Features of time-series solution

Time series solution for the scattering component can be generated using (6). We can write (6) compactly as

$$v \cong \sum_{l=1}^{N} Q(r - d_l - ct)\,, \qquad (19)$$

where

$$d_l = r - |\mathbf{r} - \mathbf{R}_l| - \delta r_l\,,$$

δr_l is given by (11) and $Q(\xi)$ is defined as

$$Q(\xi) = \mathrm{Re}\sum_m (-i)^{m+1}\frac{P_m(\cos\theta)}{\pi r} Q_m(\xi)\,.$$

Function $Q(\xi)$ describes the contribution from an individual scatterer. In a regular non-resonance case, if we ignore a time delay, its shape is similar to that of $f(\xi)$. When the carrier frequency is a resonance frequency, $Q(r\text{-}ct)$ exhibits a different behaviour typically [12] characterised by a long trail of oscillations, which occur after arrival of the main part of the response. The corresponding time series plots for these two kinds of behaviour are shown in Figure 5. These plots were obtained for a configuration given in the table and a model pulse (8) with b=2m and $a=\omega_0/c$, where ω_0 is the carrier frequency in radians. In the simulation, we used R_0=1000m, r=1000m and $\theta = 0°$.

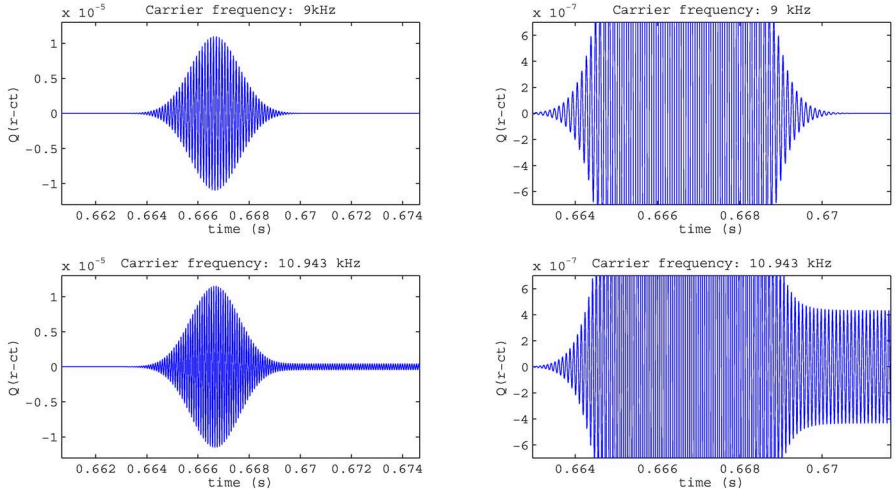

Figure 5. Transient scattering on a single shell for a resonance and non-resonance frequencies.

If we wish to obtain a collective transient scattering response from spatially distributed scatterers, we have to carry out summation of time-shifted terms (19). For our example, the result for a receiver located at (0, 0,-1000m) is shown in Figure 6.

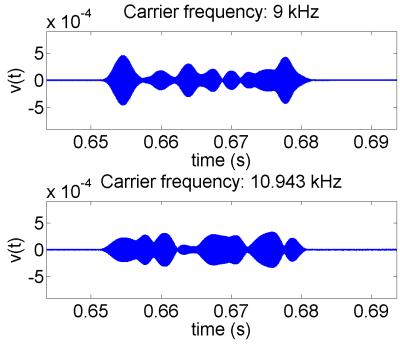

Figure 6. Examples of backscattering

The simulation in this example used 10^4 scatterers uniformly and randomly distributed in the cube $-H/2 < x, y, z < H/2$, where H was set to 20 m.

Suppose now that we have N scatterers distributed in a compact volume which is centred at the origin. An active sonar emits a pulse and tries to detect a return echo from a target. In the far-field case, contributions from scattering in the forward direction add coherently to the propagating pulse and effectively change its shape. A target located at some point (0, 0, z) will be insonified by the combined field

$$S_N(z,t) = \frac{R_0}{R_0 + z} f(z - ct) + NQ(z - ct),$$

where N is the number of scatterers and z is assumed to be positive. If the far-field conditions are not satisfied, the forward scattering will be weaker but still much more intense than the scattering in the backward direction. The diagram in Figure 7 illustrates this.

In order to obtain a crude estimate of the pulse distortion resulting from scattering and its dependence on N, we can use the ambiguity function

$$\chi_N = \frac{\int f(z - c(t+\tau)) S_N(z,t)\, dt}{\|f(z-ct)\| \, \|S_N(z,t)\|}, \qquad (20)$$

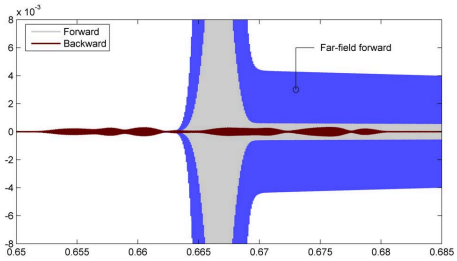

Figure 7.Comparison of scattering responses

and consider its maximum $\mu \equiv \max_\tau \chi_N(\tau)$ as a function of N. In (20), $\|\cdot\|$ denotes the root mean square operation with respect to time.

When N is not large, the value of $\mu(N)$ is very close to unity, which corresponds to little distortion. As N increases, $\mu(N)$ may decrease, and the changes are mainly noticeable in the resonance case. Simulations for the pulse and geometry under consideration show that these changes are approximately 3% if $N = 5 \cdot 10^5$. This result depends on a particular configuration and shape of the pulse. In the two-way transmission case we also have to take into account the circumstance that the scattering occurs twice, which makes the resulting change increase. There are limitations on the value of N that can be used for the above calculations. If we use 1/(fish length)^3 as an estimate of the fish density in a school [13], and assume that the scatterer specified in Table 1 corresponds to a fish length of 20 cm, then the reasonable upper estimate of possible N in a 20 m cube would be 10^6. There are

also restrictions on the use of the single scattering approximation, for the same school fish density the error of this approximation being larger at higher frequencies where the outer viscous shell becomes less transparent for the propagating sound field. Properly accounting for the effects of multiple scattering is outside the scope of this paper. However, when the concentration of fish is very high, volume shape models for entire fish schools may be used as an approximation.

In the example below we give a summary of simulation using a frequency-modulated pulse which has a smaller central frequency value (6 kHz) and a longer duration. Pulse duration and pulse bandwidth were set in this simulation to 1 sec and 200 Hz. The source location was $(0,0,1\,\mathrm{km})$, and the locations of the receiver were set to $(0,0,\pm 1\,\mathrm{km})$. The number of scatterers N was set to 10^4, they were uniformly distributed in the volume $|x|,|y|<2.5\mathrm{m}$ and $|z|<10\mathrm{m}$. The inner and outer radii of the shell were set to approximately 2 cm and 12 cm, values of the other shell parameters were the same as in Table 1. The resulting configuration has a resonance frequency in the middle of the frequency band of the considered FM-pulse.

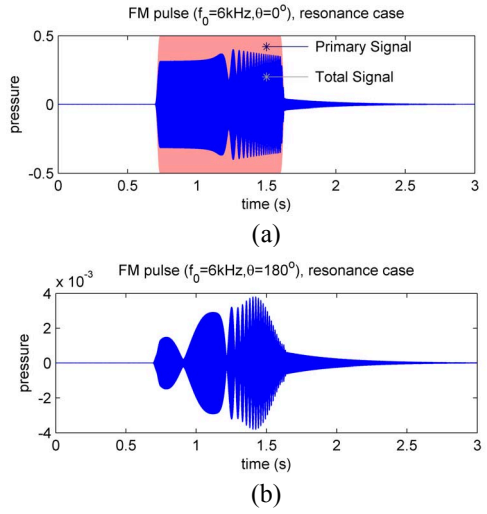

Figure 8. Time series for a 6 kHz FM-pulse

Figure 8 (a) shows a noticeable difference between the shapes of the primary and total signal. However, this distortion has very little effect on the maximal value of the ambiguity function. Its decrease is just a little more than 2% with a bias $|c\tau_{\max}|$ of about 25 cm. For the backscattering example shown in Figure 8 (b) the maximum value of the ambiguity function is 0.73. For higher frequencies and same pulse duration/bandwidth this value would be smaller due to greater phase differences of separate returns.

Conclusions

In this work we used a compressible viscous spherical shell model to simulate a collective transient scattering response of marine organisms which have gas inclusions. Evaluation of scattering parameters of individual scatterers in frequency domain has been implemented in MATLAB, access to the model's input parameters being provided via a graphical user interface.

The transient response from spatially distributed scatterers was obtained in the single scattering approximation. Features of the time series solution were analysed and interference of the forward scattering with the propagating pulse is assessed for particular types of pulses.

References

[1] Andreeva IB, "Scattering of sound by air bladders of fish in deep sound-scattering ocean layers" *Sov. Phys. Acoust*., 10:17-20, 1964.

[2] Weston DE, "Sound propagation in the presence of bladder fish" in *Underwater Acoustics*, edited by V.M.Albers, Plenum, New York, 1967.

[3] Hall M, "Volume backscattering in the South China Sea and the Indian Ocean", *J. Acoust. Soc. Am.*, 50:940-945, 1971.

[4] Love RN, "Resonant acoustic scattering by swim-bladder-bearing fish", *J. Acoust. Soc. Am.*, 64:571-580, 1978.

[5] Clay CS, "Low-resolution acoustic scattering models: fluid-filled cylinders and fish with swim bladders ", *J. Acoust. Soc. Am.*, 89:2168-2179, 1991.

[6] Stanton TK, Chu D, Wiebe PH, Martin LV, Eastwood RL, "Sound scattering by several zooplankton groups (Parts I and II)", *J. Acoust. Soc. Am.*, 103:225-253, 1998.

[7] Feuillade C, Love RH, Werby MF, "Characteristic resonance signatures for acoustical scattering from fish", *Proc. SPIE*, 2234:120-126, 1994.

[8] Ye Z, "Low-frequency acoustic scattering by gas-filled prolate spheroids in liquids", *J. Acoust. Soc. Am*., 101(4), 1997.

[9] Ding L, "Direct laboratory measurement of forward scattering by individual fish", *J. Acoust. Soc. Am*., 101(6), 1997.

[10] Feuillade C, Nero RW, "A viscous-elastic swim-bladder model for describing enhanced-frequency resonance scattering from fish", *J. Acoust. Soc. Am*., 103(6), 1998.

[11] Medwin H, Clay CS, *Fundamentals of Acoustical Oceanography*, Academic Press, Boston, 1998.

[12] Gaunaurd GC, Strifors HC, "Frequency- and time-domain analysis of the transient resonance scattering resulting from interaction of a sound pulse with submerged elastic shell", *IEEE Transactions on Ultrosonics, Ferroelectrics, and Frequency Control*, 40(4), July 1993.

[13] Lurton X, *An Introduction to Underwater Acoustics: Principles and Applications*, Springer, London, 2002.